

Compressive behavior of stretched and composite microlattice metamaterial for energy absorption applications

Mahmoud M. Osman^{a,*}, Mostafa Shazly^b, Ehab A. El-Danaf^a, Parastoo Jamshidi^c, Moataz M. Attallah^c

^a Mechanical Design and Production Department, Cairo University, Giza, 12613, Egypt

^b Mechanical Engineering Department, Faculty of Engineering, The British University in Egypt, Al-Shorouk City, Cairo, 11873, Egypt

^c School of Metallurgy and Materials, University of Birmingham, Edgbaston, Birmingham, B15 2TT, UK

ARTICLE INFO

Keywords:

Micro-lattice metamaterials
Hybrid
Selective laser melting
Finite element analysis
Energy absorption
Split Hopkinson bar testing

ABSTRACT

A new proposed truss lattice metamaterial is introduced and compared with the conventional octet truss lattice (OTL) material with regards to specific energy absorption (SEA) and energy absorption efficiency (EAE). The proposed lattice architecture resembles the Face-Centered Cubic (FCC) metamaterial with a mesostructural unit cell with an aspect ratio of 1:1:2, referred to as the stretched cell lattice (SCL). SCL and OTL samples were fabricated from stainless steel 316L by selective laser melting (SLM). Quasi-static compression experiments on the SLM fabricated metamaterials revealed an unstable twisting deformation mode for the SCL, whereas a stable crushing behavior was observed for the OTL. SCL samples provided higher SEA and EAE than OTL by 26% and 17%, respectively. Additionally, it was shown analytically, numerically and experimentally that the yield strength of the proposed SCL is ~80% higher than that of the OTL metamaterials of the same base material and relative density. A hybrid composite lattice structure based on acrylic matrix and the additively manufactured microlattice metamaterials was produced to enhance the struts buckling resistance. The hybrid composite showed a 47% higher specific strength while the SEA and EAE dropped by 31.5% and 30.7%, respectively, when compared to the bare stainless steel microlattice. Dynamic compression experiments using Split Hopkinson Pressure Bar (SHPB) at strain rates in the order of $10^3/\text{s}$ demonstrated a similar deformation plateau as the static compression experiments with a dynamic increase factor (DIF) of ~1.3 for the bare stainless steel metamaterials and ~2 for the acrylic-stainless steel hybrid composite material.

1. Introduction

Mechanical metamaterials are man-made structures whose mechanical properties can be manipulated by changing their geometric structure [1,2] and via architected microstructure [3,4]. Their mechanical properties can be engineered to possess exceptional values that cannot be found in nature. Recently, there are wide range of new emerging materials that can be included under this definition such as: pentamode materials, auxetic materials, materials with negative mechanical constitutive coefficients, and materials with enhanced mechanical properties [5]. Truss lattice materials can be considered as mechanical metamaterials where their mechanical properties are dependent on the architecture of their mesostructure unit cell and the properties of the parent material from which they are fabricated. In particular, truss lattice structures are comprised of a unit cell that is

periodically repeated in the three directions forming a lattice material that can be considered as a homogenous solid at the macro-scale. Each unit cell is fundamentally composed of trusses (struts) stacked with different arrangement and air occupies most volume [6]. Accordingly, truss lattice materials fall under the category of artificial cellular materials such as foams, and honeycombs. As a cellular material, lattice structures feature lightweight, high specific strength and stiffness, large surface area to volume ratio, which allows for their use in thermal insulation, filtration and separation, load bearing and energy absorption applications [4,6–8].

The design of lattice materials for energy absorption applications has been previously reported [4,9–13]. The truss lattice, similar to foams and honeycombs, collapses progressively under uniaxial compressive loads and the macroscopic stress-strain response features a constant plateau stress from initial yield till densification stage [13–15]. Their cellular

* Corresponding author.

E-mail address: mahmoud-magdy@cu.edu.eg (M.M. Osman).

nature provides high compressibility up to high strains prior to densification which allows for high energy absorption capacity and alleviating impulsive loads by extending their duration. Recent advancements in metal additive manufacturing (AM) techniques have enabled the fabrication of metallic truss lattice structures with any complex topology whose dimensions close to the microscale. Metallic microlattices have been built by electron beam melting (e.g. Ref. [16]) and by selective laser melting (SLM) (e.g. Refs. [17,18]).

Many studies are performed on SLM fabricated metallic microlattice structures for energy absorption applications using numerical and experimental approaches. Vrana et al. [19] tested a four series of BCC microlattice, that resembles body-centered cubic cell, under impact with a spherical indenter, and reported that the BCC with a strut diameter of 0.8 mm to have the best combination of stiffness and energy absorption. Tancogne-Dejean et al. [20] studied the effect of tapering the constituent struts of BCC metamaterial on the elastic response and the specific energy absorption (SEA) capacity. Their theoretical analysis and numerical simulations showed an increase in the effective Young's modulus and SEA up to 70% and 45%, respectively, which were validated experimentally on SLM specimens fabricated from stainless steel 316L. Tancogne-Dejean et al. [21] performed a parametric study through finite element (FE) simulations to examine the effect of the relative density and truss cross section of octet truss (FCC) lattice on the energy absorption characteristics. Contuzzi et al. [22] explored the effect of cell size and strut size while adding a vertical reinforcement to the pillar textile microlattice fabricated from 18Ni Marage 300, and found the lattice specific strength to increase. Harris et al. [23] created a hybrid geometry by combining square honeycomb and lattice architecture in which the cell walls of the square honeycomb are replaced by a truss lattice of the same relative density and found it to outperform square honeycomb.

There has been a considerable amount of work developing analytical formulas for the mechanical behavior of some mechanical metamaterials architectures. Analytical expressions of the strength and stiffness of octet truss cell were previously derived by Deshpande et al. [24] and Johnston et al. [25]. Their analytical models assume an elastic-perfect plastic material, pin-jointed struts, and a stretching dominated structure. Deshpande et al. [26] investigated the typological criterion that differentiates between stretching dominated and bending dominated lattice structured materials, based on the number of the mesostructure cell struts and nodes, and found that the stretching dominated lattices are more weight efficient. Elsayed et al. [27] designed selection charts for the design of the octet-truss lattice, so that the plastic yielding and elastic buckling of the cell struts occur simultaneously by shaping cell element cross section area. Ushijima [28] presented a theoretical analysis for predicting stiffness and plastic yielding of BCC metamaterial which were verified against FE and experimental results.

Composite structures based on cellular materials has been studied recently aiming at increasing their SEA. This has been done by filling the free spaces of cellular materials, such as: foams, honeycombs, and lattice materials, with polymers. Cluff et al. [29] investigated the static and dynamic compressive behavior of hybrid material composed of aluminum foam filled with a thermoplastic polymer. They found that the hybrid material features higher strength and energy absorption capacity compared with the aluminum foam and the polymer individually over wide range of strain rates. Liu et al. [30] studied the effect of filling aluminum honeycomb with Expanded Polypropylene (EPP) foam on its axial and lateral crushing responses. Foam filled honeycombs absorbed higher total energy than the sum of bare honeycomb and foam separately under axial and lateral loadings, whereas the SEA remained unchanged for axial loading but increased significantly during lateral crushing. The dynamic response of the same hybrid material is studied experimentally and numerically by Zhang et al. [31]. At the same impact velocity, foam filled honeycombs had higher peak and mean strength while the deformation stroke and the SEA decreased significantly compared to the bare honeycomb. Zhang et al. observed a substantial

increase in the SEA by 68% and 152% with the increase of the impact velocity from 2 m/s to 2.6 m/s and 3.2 m/s respectively. Campbell et al. [32] studied the effect of reinforcing tetrahedral and pyramidal architectures fabricated from perforated 3003 Aluminum alloy sheets with rigid Polyurethane foam. These hybrid materials offered a comparable stiffness and 59% higher strength when compared with their corresponding components. Yungwirth et al. [33] conducted a series of experiments to study the ballistic behavior of hybrid material based on pyramidal truss cores fabricated from stainless steel by perforated sheet folding process, and filled by various ceramic and polymeric inserts, which provided greater resistance to penetration.

In literature, few studies were concerned about the use of microlattice structures as a basis for a hybrid composite structure. A hybrid composite material, based on additively manufactured BCC microlattice made from stainless steel 316L and rubber-like material, was developed by Gümruk et al. [34]. The hybrid material composed of small cell size lattice had significantly enhanced energy absorption and plateau stress. On the other hand, the composite material with larger cell size, suffered from a monotonic stress increase at very low densification strain, with no clear plateau regime, which negatively influenced the energy absorption characteristics, while can be beneficial in increasing projectile penetration resistance. Gümruk et al. did not compare the SEA of the hybrid material to that of the bare stainless steel microlattice [34].

The present study aims at evaluating the energy absorption of a lattice architecture similar to the FCC lattice but with different mesostructure unit cell aspect ratio fabricated by SLM from stainless steel 316L. These proposed lattice samples were tested under uniaxial compression at strain rates ranging from quasi-static up to the order of $10^3/\text{s}$. The deformation behavior was studied for both conventional and proposed architectures through numerical simulations and validated through experimental results. In addition, a hybrid composite structure based on the proposed stainless steel microlattice and a space-filling acrylic material, was introduced and tested at the same strain rates, whereby the effect of this hybridization on SEA, energy absorption efficiency (EAE) and specific strength is evaluated.

2. Analytical analysis

The relative density of the lattice ($\bar{\rho}$) is defined by the ratio of the lattice macroscopic density (ρ_l) to the density of the basis material (ρ_s) which is equivalent as well to the ratio between the volume of the lattice trusses to the volume of the bulk cell.

$$\bar{\rho} = \frac{\rho_l}{\rho_s} \quad (1)$$

Using an approximate analytical relationship, the relative density ($\bar{\rho}_{OTL}$) of the octet truss lattice (OTL) with cylindrical struts of radius R and length L , shown from different perspectives in Fig. (1a, and 1b), is given [24,27]:

$$\bar{\rho}_{OTL} = 6\sqrt{2}\pi \left(\frac{R}{L}\right)^2 \quad (2)$$

Eq. (2) overestimates the relative density due to double counting the volume of nodes. A higher-order approximation of the relative density is given by:

$$\bar{\rho}_{OTL} = 6\sqrt{2}\pi \left(\frac{R}{L}\right)^2 - C \left(\frac{R}{L}\right)^3 \quad (3)$$

where C is a coefficient that depends on the detailed geometry of the nodes. Fitting the relative densities calculated from solid modelling software suggests the coefficient C to be 54.6 [21]. The equation can be rewritten as a function of the cell edge length (a) as:

$$\bar{\rho}_{OTL} = 12\sqrt{2}\pi \left(\frac{R}{a}\right)^2 - C \left(\frac{R}{a}\right)^3 \quad (4)$$

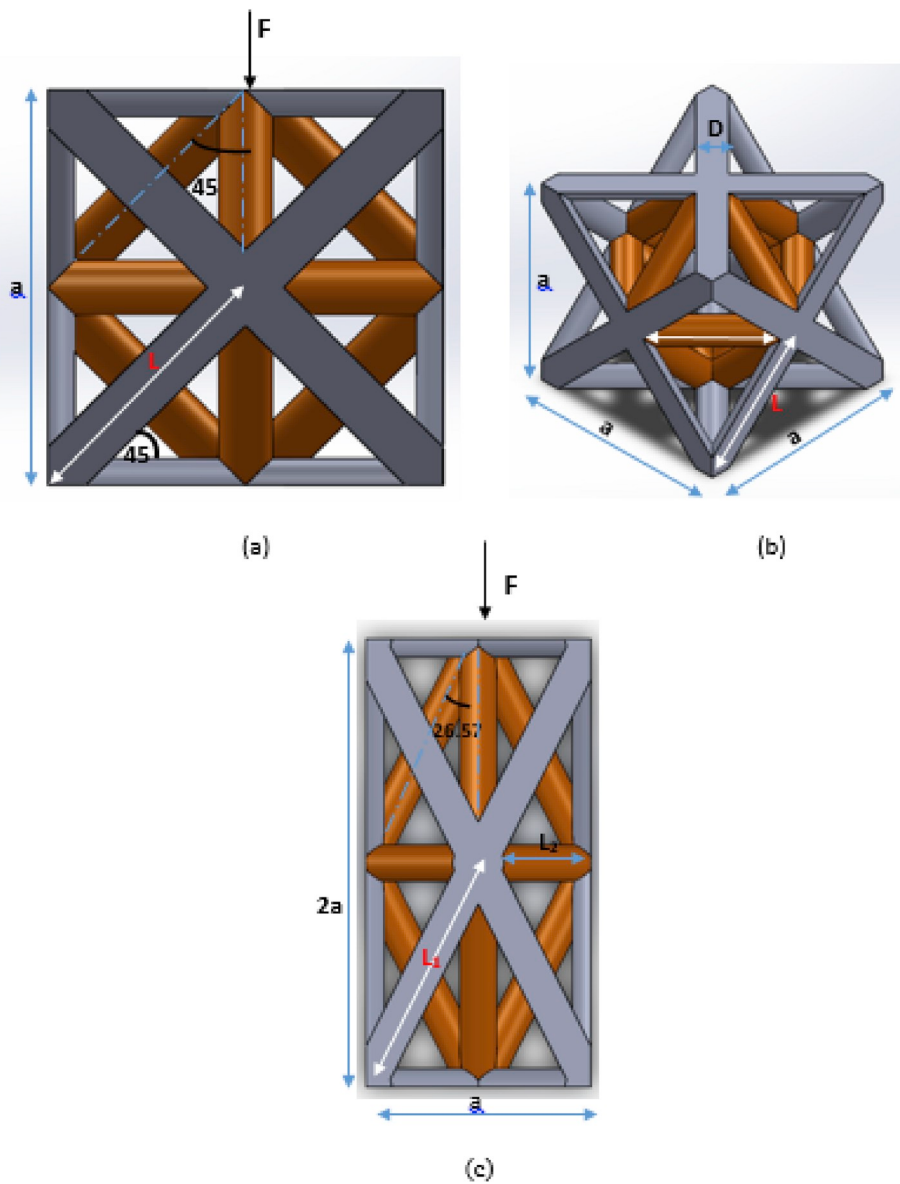


Fig. 1. A unit cell of the OTL (a, and b) and the SCL (c) with major dimensions $a = 3.08$ mm, $L = 2.18$ mm.

with coefficient $C = 154.4$.

Similarly, the relative density ($\bar{\rho}_{SCL}$) of the stretched cell lattice (SCL) which features different cell aspect ratio and of cell edge lengths (a : a : $2a$), presented in Fig. 1c, is given by:

$$\bar{\rho}_{SCL} = \left(4\sqrt{5} + 2\sqrt{2}\right)\pi\left(\frac{R}{a}\right)^2 - C\left(\frac{R}{a}\right)^3 \quad (5)$$

The coefficient C is found to be 88.8, based on fitting density obtained from solid modelling software.

The lattice structure generally fails due to either buckling or yielding of the constituent struts under uniaxial compression. The following assumptions are made: (1) the material is elastic-perfect plastic with a yield strength (σ_y) for the lattice; (2) a stretching-dominated structure i.e. only axial loads are considered; and (3) the octahedral cell only is considered (the brown colored (dark) part of the truss in Fig. 1). By simple force analysis, the yielding force of the OTL (F_{y11}), shown in Fig. 1a, can be deduced from the yielding force of its constitutive struts (F_{ys1}) as follows:

$$F_{y11} = 4F_{ys1} \cos(45^\circ) \quad (6)$$

The yielding force of the struts of the OTL can be expressed as follows:

$$F_{ys1} = \sigma_y \frac{\pi}{4} (D_1)^2 \quad (7)$$

where D_1 is the diameter of the constitutive struts of the OTL and σ_y is the yield strength of the basis material.

Similarly, the yielding force (F_{y12}) of the SCL, which has an aspect ratio of (1:1:2) i.e. the cell edge in the Z-direction (direction of loading) is doubled as shown in Fig. 1c, can be deduced from the yielding force of its constitutive struts (F_{ys2}) as follows

$$F_{y12} = 4F_{ys2} \cos(26.57^\circ) \quad (8)$$

$$F_{ys2} = \sigma_y \frac{\pi}{4} (D_2)^2 \quad (9)$$

where D_2 is the diameter of the constitutive struts of the SCL.

The ratio of the yielding forces $\left(\frac{F_{y12}}{F_{y11}}\right)$ of the SCL to the OTL can be calculated based on Eqs. (6)–(9), while assuming the same basis material

for both models.

$$\frac{F_{yl2}}{F_{yl1}} = \frac{\cos(26.57^\circ)}{\cos(45^\circ)} \left(\frac{D_2}{D_1}\right)^2 = \frac{2\sqrt{10}}{5} \left(\frac{D_2}{D_1}\right)^2 \quad (10)$$

Since both cubic cell and stretched cell models have the same apparent area (a^2), the ratio of the yield strength of the SCL to that of the OTL $\left(\frac{\sigma_{yl2}}{\sigma_{yl1}}\right)$ can be expressed as follows:

$$\frac{\sigma_{yl2}}{\sigma_{yl1}} = \frac{\cos(26.57^\circ)}{\cos(45^\circ)} \left(\frac{D_2}{D_1}\right)^2 = \frac{2\sqrt{10}}{5} \left(\frac{D_2}{D_1}\right)^2 \quad (11)$$

The ratio depends on the inclination angle of the struts to the vertical direction (applied force direction) and the constituent struts diameters of each model. The basis material is assumed to be the same for both models. The inclination angle of the struts is 45° for the OTL and 26.57° for the SCL as shown in Fig. 1a and c.

These microlattice structures were studied for energy absorption purposes; thus, we used two metrics to measure their performance; namely, EAE and SEA. EAE (η) is defined as the actual energy absorbed by the lattice up to the point of densification, to the maximum possible energy absorbed which is assumed to be obtained at a constant crushing strength (σ_{tr}) from 0 to 100% strain and is expressed as [35]:

$$\eta = \frac{\int_0^{\epsilon_D} \sigma d\epsilon}{\sigma_{tr} * 100\%} \quad (12)$$

where σ is the compressive stress and ϵ is the compressive strain; σ_{tr} is the transmitted stress and ϵ_D is the densification strain.

SEA is defined as the energy absorbed by material subjected to uniaxial compression per unit mass. The SEA is expressed as follows:

$$SEA = \frac{\int_0^{\epsilon_D} \sigma d\epsilon}{\rho_l} \quad (13)$$

where ρ_l is the macroscopic density of the lattice structure.

3. Experimental procedure

3.1. Additive manufacturing of micro-lattices

Micro lattice parts were fabricated from stainless steel 316L gas atomized powder (Atomizing Systems Ltd, UK) sized 15–45 μm using Concept Laser M2 Cusing SLM machine. The machine is equipped with a 400W fiber laser operated in continuous wave mode. The adopted process parameters are summarized in Table 1. These process parameters along with a laser beam of 60 μm diameter spot size were used in fabricating all samples which eliminates the effects of the process parameters in the present work.

The two models, OTL and SCL were manufactured and presented in Fig. 2 (a, b, c) for OTL and in Fig. 2 (d, e, f) for SCL. For each model two sizes were fabricated; one for quasi-static testing with dimensions of $\sim 12.32 \times 12.32 \times 10.78 \text{ mm}^3$ shown in Fig. 2 (a and d) and the second for dynamic testing with dimensions of $\sim 12.32 \times 10.78 \times 6.16 \text{ mm}^3$ for OTL (Figs. 2c) and $12.32 \times 12.32 \times 4.1 \text{ mm}^3$ for the SCL (Fig. 2f). The reason for decreasing the sample thickness is to be suitable for dynamic testing on Split Hopkinson Pressure Bar (SHPB). The OTL was designed to have a cell size of 3.08^3 mm^3 , whereas the SCL has a periodic cell of $3.08 \times 3.08 \times 6.16 \text{ mm}^3$, which corresponds to a cell aspect ratio of

(1:1:2) where the cell edge length is doubled in the load direction. The designed constituent strut diameters of the OTL and the SCL were 420 μm and 503 μm , respectively. This is to ensure a designed relative density of 0.2 for both models. A relative density of 0.2 was selected based on a previous FE parametric study, performed on the same proposed microlattice configuration, showing that the best combination of SEA and EAE is obtained at this relative density. The best relative density was selected based on a decision matrix that gives equal weight factor for both SEA and EAE [36].

Mini-cylinder specimens (micro-struts) with 500 μm diameter and 30 mm long built in a direction parallel to their axes were used for the purpose of material characterization and providing the constitutive response of the SLM fabricated material. They were fabricated with a diameter similar/close to the constituent diameters of the fabricated lattices, because the strength of the basis material fabricated by SLM is size dependent as revealed by Tancogne-Dejean et al. [21].

3.1.1. Hybrid stainless steel 316L microlattice impregnated with acrylic thermoplastic

A QuickSet Acrylic (provided by Allied High Tech) was prepared by mixing the acrylic powder to the liquid hardener with a mixing ratio 2:1 by volume. It features a fast curing time (6–10 min), very low shrinkage, and good edge retention. After mixing the acrylic powder and the liquid hardener, the produced mixture was poured and pressed on the SLM fabricated lattices to fill the spaces within the lattice. Images of the hybrid composite structures are presented in Fig. 3a for the SCL and Fig. 3b for the OTL.

3.2. Material characterization

The density of the basis material of the built specimens was measured by hydrostatic weighing that is based on Archimedes' principle. The weight of the lattices are measured in air and in methanol. Using Eq. (14) [37], the density of the basis material was calculated which could indicate the percentage of porosity inside the structure, if compared with the density of stainless steel 316L reported in the literature. The density of the lattice basis material (stainless steel 316L) made by SLM is denoted by (ρ_{ss}) and calculated from the following equation:

$$\rho_{ss} = \frac{m_a * \rho_m - m_m * \rho_a}{m_a - m_m} \quad (14)$$

where m_a , m_m are the mass of the lattice in air and in methanol respectively and ρ_a , ρ_m are the density of the air and methanol respectively.

A polarized light microscope (Eclipse LV100 POL) from Nikon, with a high intensity 50W halogen light source and equipped with a high-definition color camera head (Nikon DS-Fi1), was used to measure the average strut diameter in the SLM fabricated lattice to be compared with its intended designed value. Images were taken on the red colored (dark) struts in Fig. 4, which can be categorized into horizontally built struts (i.e. the build direction is perpendicular to the strut axis) and inclined struts to the build direction by 45° for the OTL and 26.5° in the SCL. Horizontal struts are located on both top and bottom faces of the lattice, while the inclined struts are on the lateral faces of the lattice. Several readings of strut diameter were taken at different positions on strut surface for both the horizontal and the inclined constitutive struts, to obtain an average value for the whole lattice constitutive strut diameter.

The outer dimensions of the fabricated lattices were measured with a 1 μm precision micrometer and their masses were measured with a 0.1 gm precision sensitive balance; therefore, the density of the specimens could be calculated. The relative density of the lattice was calculated by taking the ratio of the lattice density to the density of the bulk stainless steel 316L reported in the literature (8 g/cm^3).

Table 1
SLM Process parameters for stainless steel 316L (Concept Laser M2).

Laser power [W]	100
Layer thickness [μm]	30
Scan speed [mm/s]	475
Hatch distance [μm]	45

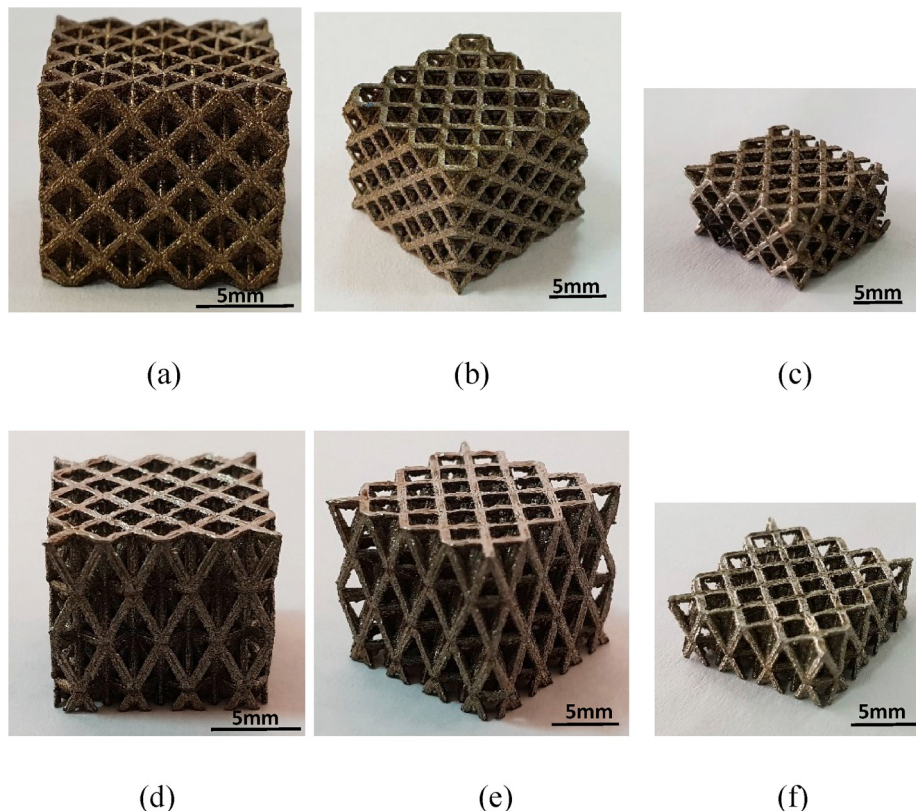


Fig. 2. Fabricated micro-lattice samples made from stainless steel 316L by SLM; (a) and (b) the OTL; (d) and (e) the SCL; (c) and (f) corresponding models for dynamic testing via SHPB.



Fig. 3. Hybrid composite structure composed of acrylic matrix and the stainless steel SCL (a) and the OTL (b).

3.3. Mechanical testing

3.3.1. Micro-strut testing

The tensile tests of the mini-cylinder specimens of 30 mm long and 500 μm diameter were carried out using a bench top tensile testing machine (SDL Atlas-H5kt), for basis material characterization. A 500 N load cell is mounted on the machine to accurately measure the micro-strut resisting forces. The test was carried out at a constant speed of 20 mm/min with a strut gage length of 10 mm which corresponds to a strain rate of $3.3 \times 10^{-2} \text{ s}^{-1}$. Four struts were tested to ensure the consistency of the results and an average stress-strain curve was extracted from the test data.

3.3.2. Lattice static compression

Stainless steel 316L bare micro-lattices, plain acrylic, and the hybrid

composite material were tested quasi-statically on a WDW-100D Electronic Universal Tensile Testing Machine with a 100 kN capacity. The static uniaxial compression experiments were performed under a constant cross-head velocity of 1 mm/min which is equivalent to a strain rate of about 10^{-3} s^{-1} . All specimens were placed between greased machine platens made of high strength steel to minimize the friction between the interaction surfaces.

3.3.3. Lattice dynamic compression

A Split Hopkinson Pressure Bar (SHPB) was used for the high strain rate experiments. The SHPB used in the present work consists of 20 mm diameter aluminum bars. The striker, incident and transmitter bars have lengths of 0.45 m, 1.58 m, and 1.78 m, respectively. The incident, reflected and transmitted signals are registered on PC-Based oscilloscope using 120Ω strain gages strategically placed on the incident and

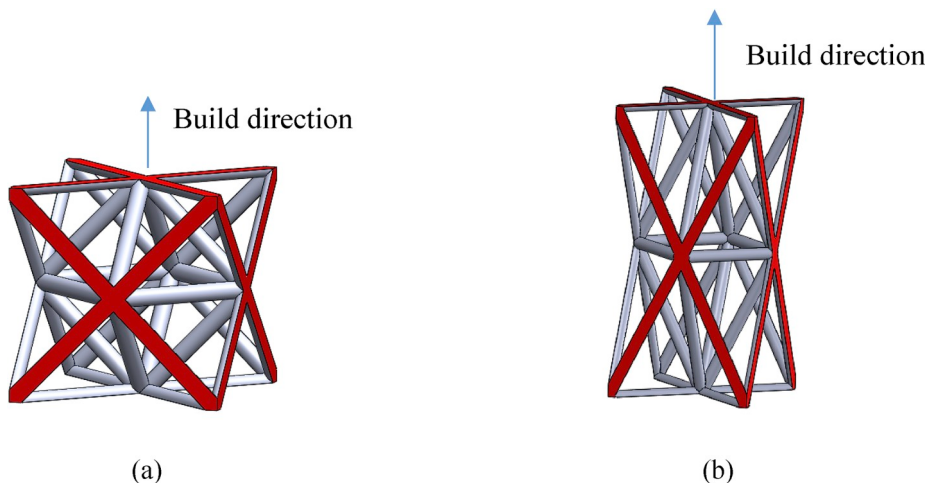


Fig. 4. Constitutive struts (red colored-dark) measured by the polarizing microscope for the OTL (a) and the SCL (b). (For interpretation of the references to color in this figure legend, the reader is referred to the Web version of this article.)

transmitter bars and connected to Wheatstone bridge. One dimensional wave analysis was used to infer stress, strain rate and strain [38].

4. Finite element modelling

4.1. Simulation model

The aim of the FE simulations is to study the large strain compressive response of the stainless steel 316L micro-lattice structures. To model the OTL and the SCL metamaterials, two approaches are used: (1) a single cell model was used and symmetric boundary conditions were applied, to capture the mesoscopic deformation mode, as shown in

Fig. (5a, and 5b); and (2) a full scale FE model with the same dimensions of the fabricated lattices was used to get the macroscopic deformation behavior and investigate the crushing progression of the whole lattice, as shown in **Fig. 5c** for the OTL and **Fig. 5d** for the SCL.

The OTL model features a strut of 420 μm diameter, **Fig. 5a**, while the SCL, **Fig. 5b**, has 503 μm diameter constituent struts allowing for an equal relative density of 0.2 for both models. The models were meshed using C3D4, a first order, four-node tetrahedral element from ABAQUS® V.6.14.1 library, with a maximum size of 70 μm determined from mesh sensitivity analysis. The models were placed between two rigid plates with 0.1 tangential coefficient of friction. The bottom rigid plate was fixed, whereas the upper plate was given a controlled displacement at

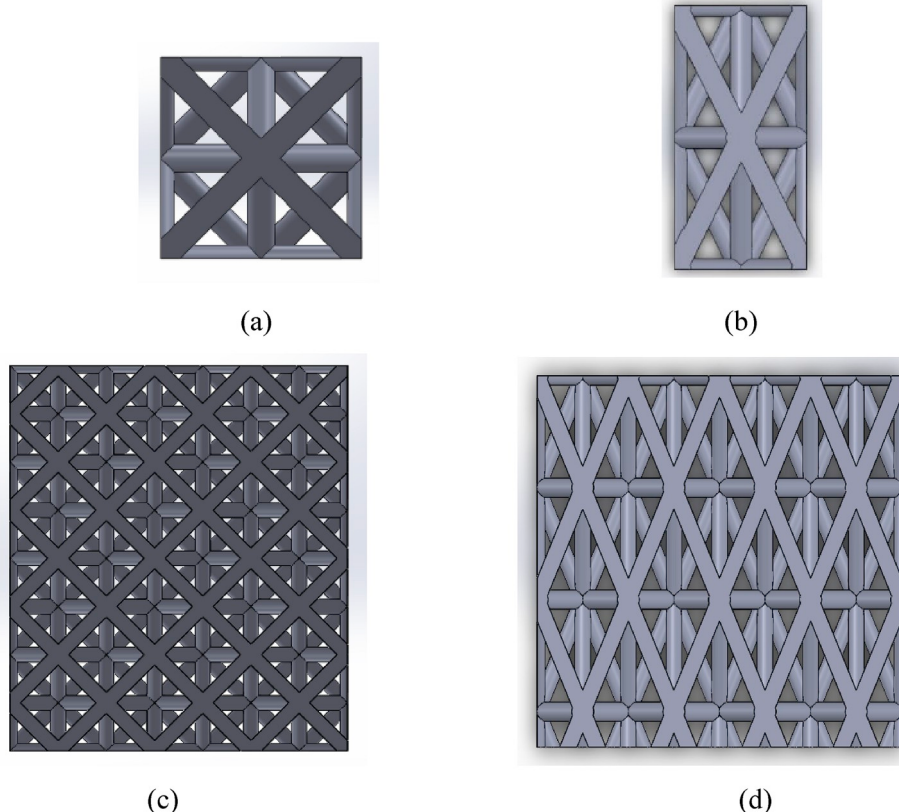


Fig. 5. The periodic cell model and the full scale model used in FE simulations for the OTL (a and c) and the SCL (b and d).

constant velocity which ensures the densification of the lattice material. The quasi-static simulations were performed using ABAQUS®/Explicit solver due to its ability to capture both material and geometrical nonlinearities and complex contact between the struts. To ensure that the inertia effects are minimal, a step time of 10^{-3} s was selected and found to produce a kinetic energy that is less than 10% of the strain energy. General contact algorithm was used to model the contact between the rigid plates and octet cell as well as between the struts during the deformation process.

4.2. Basis material modelling

At a preliminary stage prior to samples fabrication, the FE model was fed with a material model reported by Tancogne-Dejean et al. [21] for stainless steel 316L fabricated by SLM and obtained from in-situ experiments on a single strut of 0.81 mm diameter. The reported yield strength at 0.2% plastic strain was 384 MPa and the large strain response was approximately linear with a tangent modulus of 1470 MPa. The results of the FE simulations based on this material model are presented in Section 5.2.

Later, a new constitutive behavior of the basis material was obtained from tensile experiments on a strut of 500 μm diameter and fabricated from stainless steel 316L with the same SLM process parameters, in Table 1, used in the fabrication of microlattice samples. The obtained basis material response is presented in section 5.4 and is fed to the FE model for comparing the anticipated FE simulation results with the results obtained from quasi-static compression experiments, which will be demonstrated in Section 5.5.1.

5. Results & discussions

5.1. Analytical formulations

Recalling Eq. (11), increasing the OTL unit cell aspect ratio to (1: 1: 2) will surely enhance the yield strength of the lattice at the same relative density ($\bar{\rho}$) and same cell length (a). This increase is basically for two reasons: (1) the inclination angle of the struts with the vertical direction; the struts in the SCL are inclined more towards the vertical direction which gives the model a substantial rise in the lattice yield strength; and (2) the increase in the constitutive strut diameter of the SCL compared with the OTL at the same relative density. It was found based on Eq. (3) and Eq. (5), that the SCL has constitutive struts of ~20%

larger than that of the OTL for any relative density for both models, as shown in Fig. 6 ($R_2/R_1 = \sim 1.2$).

Based on Eq. (11), the ratio between the yield strength of the SCL and that of the OTL was calculated and plotted in Fig. 6 for a range of relative densities from 0.05 to 0.7. It was found analytically that the yield strength of the SCL is ~80% higher than that of the OTL at the same relative density ($\bar{\rho}$), cell length (a), and lattice basis material, as revealed in Fig. 6 ($\frac{\sigma_{y2}}{\sigma_{y1}} = \sim 1.8$).

5.2. Finite element simulations

5.2.1. Microlattice compressive response

FE simulations, based on the material model provided by Tancogne-Dejean et al. [21], of both the OTL model and the SCL revealed the superiority of the SCL over the OTL in terms of the lattice yield strength and energy absorption capabilities as shown in Fig. 7. The yield strength of the OTL is 29 MPa, while the SCL has a strength of 59 MPa, this yield to a ratio of $\frac{\sigma_{y2}}{\sigma_{y1}} = 2$, which means 100% increase in the yield strength for the SCL. However, analytical results showed only a percentage of 80% increase, this could be attributed to the tetrahedral cell effect; since, the analytical model only considered the octahedral cell of the FCC cell. The diameter of the constitutive struts of the tetrahedral cell and their inclination to the vertical direction in case of the SCL enhances the yield strength of the lattice. The SEA of the SCL was calculated from Eq. (13) based on the resulting stress strain curve from FE simulations shown in Fig. 7, and found to be 46.3 kJ/kg, in contrast to 21.6 kJ/kg for the OTL. In addition, the EAE for the SCL and the OTL are 46.3% and 54.3%, respectively. The EAE for the two models did not change significantly, although the SEA increased for the SCL almost to double its value for the conventional OTL.

5.2.2. Deformation mechanism

The OTL features a stable deformation mode. Plastic hinges are formed at struts intersections (nodes) as shown in Fig. 8a. However, the OTL features a stable, uniform deformation mode as shown in Fig. 8a at the mesoscopic unit cell level and Fig. 8c for the full scale macroscopic lattice level. Equivalent plastic strain contours are given in Fig. 8a and b for both models showing the localized plastic strain at strut intersection for the OTL (Fig. 8a) and at the strut center in the SCL (Fig. 8b). On the other hand, the constitutive struts of the SCL buckle under uniaxial compression due to their low strut diameter normalized by their lengths

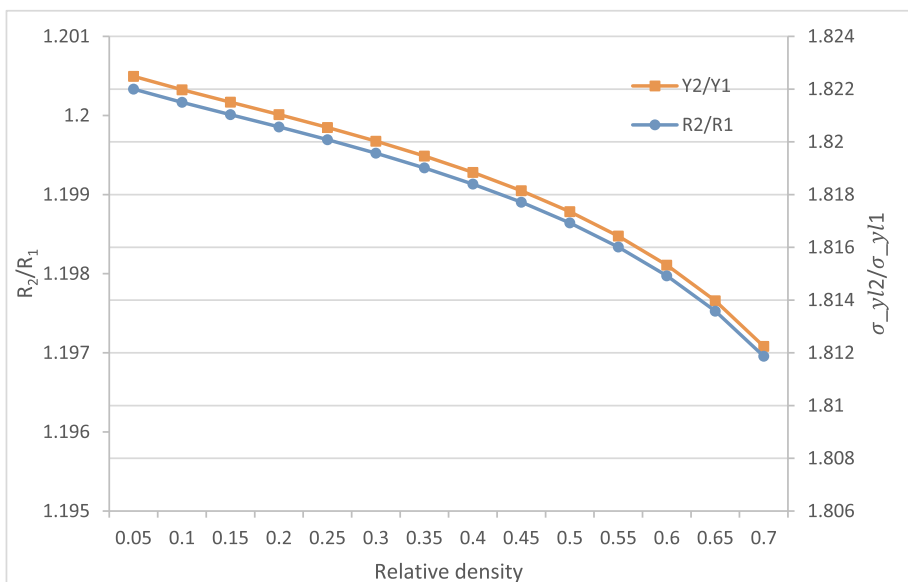


Fig. 6. Radius and yield strength ratios of the SCL to the OTL with relative density.

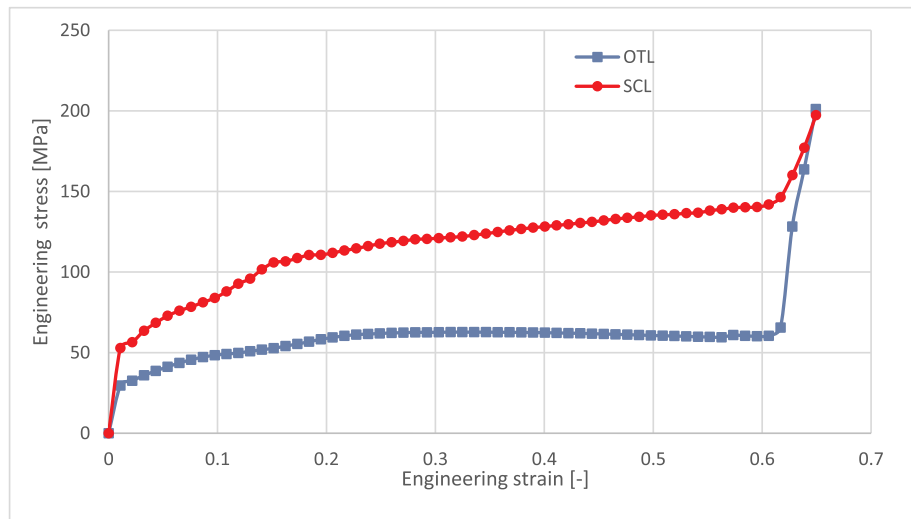


Fig. 7. Macroscopic stress strain curve of a unit cell of OTL and SCL based on FE simulations.

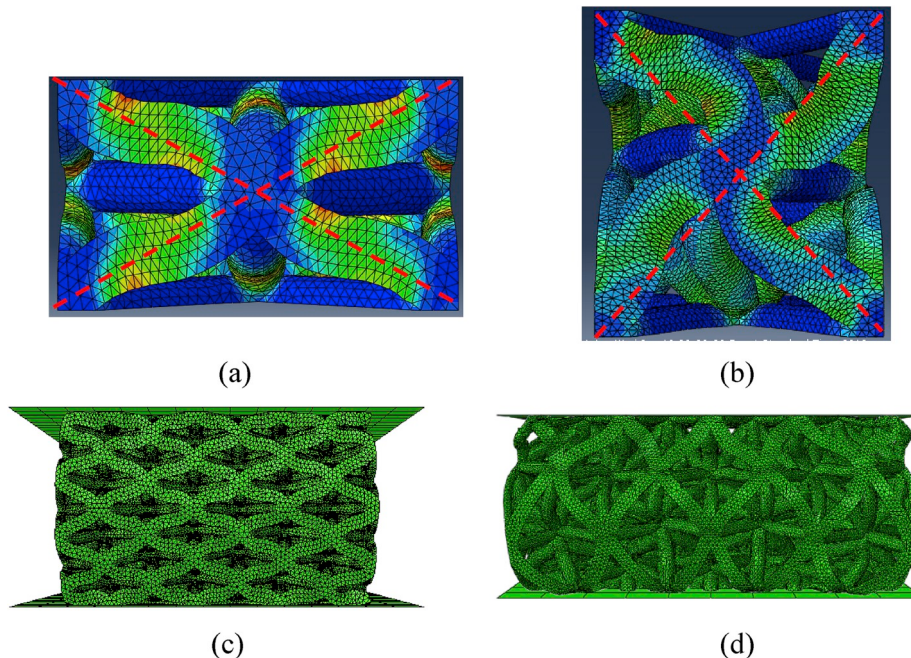


Fig. 8. Mesoscopic deformation modes of the OTL (a) and the SCL (b) and the macroscopic deformation of the OTL (c) and the SCL (d).

(D/L). Besides the plastic hinges formed near nodes, additional plastic hinges are formed near the centers of the struts. During further compression of the lattice, plastic deformation is concentrated more at strut center, while strut intersections (nodes) feature a rigid body rotation resulting in lattice twisting (twist mode). The deformation mechanism of the SCL is unstable twisting mode as shown in Fig. 8b (mesoscopic level) and Fig. 8d (macroscopic level).

5.3. Microlattice samples assessment

5.3.1. Density measurements

The percentage of porosity in the SLM fabricated lattice samples was indicated by hydrostatic weighing technique which is based on Archimedes' principle. The weight of the lattice was measured in air and in methanol and; thus, the density of the lattice basis material was determined by Eq. (14). The density of the basis material of the fabricated lattices was found to be 7954 kg/m^3 compared to 8000 kg/m^3 , reported

in the literature for the stainless steel 316L, which indicates a micro-porosity of $\sim 0.6\%$ in the built specimens. The percentage of porosity can be controlled by adjusting SLM process parameters which will reflect on the build integrity.

The outer dimensions, mass and density of both OTL and SCL metamatamaterials are given in Tables 2 and 3, respectively. From a sample of seven specimens, the OTL had a relative density of 0.274 with a standard deviation of 0.7%, while the average relative density of the SCL was 0.227 with a standard deviation of 0.2%. For a target relative density of 0.2, it is clear that the manufacturing accuracy of the proposed SCL is higher than that of the OTL using the same SLM process parameters. This is attributed to the inclination angle of the lattice constituent struts to the build direction.

The density of the stainless steel-acrylic composite material was measured for both models and compared with the density of their corresponding bare stainless steel lattice. The composite SCL had a measured density of 2.3 g/cm^3 (30% increase) compared to the density

Table 2

Fabricated OTL physical data.

	x-direction [mm]	y-direction [mm]	Build direction [mm]	Mass [g]	Density [g/cc]	Relative density [-]
Average	12.519	12.526	10.73	3.69	2.192	0.274
Std. dev	0.012	0.014	0.300	0.069	0.056	0.007

Table 3

Fabricated SCL physical data.

	x-direction [mm]	y-direction [mm]	Build direction [mm]	Mass [g]	Density [g/cc]	Relative density [-]
Average	12.528	12.536	10.748	3.071	1.819	0.227
Std. dev	0.03	0.039	0.227	0.076	0.016	0.002

of the bare stainless steel SCL of 1.819 g/cm^3 . The composite OTL had a density of 2.48 g/cm^3 (14% increase) compared to the stand-alone OTL of 2.192 g/cm^3 . The density of the used QuickSet Acrylic was measured to be 1.15 g/cm^3 compared to the known acrylic (PMMA) which has a density of 1.18 g/cm^3 according to DIN 53479 [39].

5.3.2. Dimensional accuracy of constitutive struts

The micro-lattice constitutive struts were measured through polarized light microscope images by recording several readings on different sections of the constitutive struts of each lattice, see Fig. 9. The resulting dimensions are presented in Table 4. The OTL featured an average strut diameter of $473 \mu\text{m}$ compared to a target value of $420 \mu\text{m}$ while the SCL had an average strut diameter of $527 \mu\text{m}$ as compared to the intended design value of $503 \mu\text{m}$, for the same SLM process parameters. The orientation of the constituent struts to the build direction influenced the dimensional accuracy of the built lattice metamaterials. As shown in Table 4, the average diameter of the horizontal constituent struts of the OTL (90° to the build direction) was found to be $449 \mu\text{m}$ whereas, the average diameter of the inclined strut (45° to the build direction) was measured to be $498 \mu\text{m}$ which is deviated more from the intended design value of $420 \mu\text{m}$.

For the SCL, the dimensional accuracy of both inclined (26.5° to the build direction) and horizontal struts were almost the same and the diameters were measured to be $530 \mu\text{m}$ and $524 \mu\text{m}$ respectively, which is not deviated much from the intended designed value of $503 \mu\text{m}$. Generally, horizontally built struts revealed good dimensional accuracy compared to the 45° inclined struts, and as the inclination angle decreases the accuracy gets better which is revealed in the 26.5° inclined struts of the SCL.

Table 4

Constitutive average strut diameters of the OTL and the SCL.

Strut	OTL	SCL
Horizontal strut [μm]	449	524
Inclined strut [μm]	498 (inclined by 45°)	530 (inclined by 26.5°)
Average value [μm]	473	527
Intended target value [μm]	420	503

5.4. Constitutive behavior of SLM fabricated struts

The true stress-strain curve obtained from the static tensile experiments of the $500 \mu\text{m}$ strut, fabricated by SLM from stainless steel 316L (SS316L), is depicted in Fig. 10. The curve features a yield strength (σ_y) of 294 MPa and an approximately linear hardening behavior with a tangent modulus of 1250 MPa , ultimate tensile strength (σ_u) of 489 MPa and 35% elongation at break (ϵ_f). From this point onward, this material model was used in FE simulations of microlattice compressive response for comparison with the experimental results obtained from quasi-static compression experiments.

By comparing the obtained constitutive behavior with the reported mechanical properties of wrought SS316L which are: $\sigma_y \geq 170 \text{ MPa}$, $\sigma_u \geq 485 \text{ MPa}$ and $\epsilon_f \geq 0.4$, based on ASTM A240/A240M28 [40], it was found that the obtained SS316L behavior in the present work is above the standard values for wrought SS316L. In addition, The SS316L material model obtained by Tancogne-Dejean et al. [21], used in the earlier section of the present work, is presented in Fig. 10 for comparison.

5.5. Quasi-static testing of microlattice

5.5.1. Bare stainless steel lattices

The quasi-static compression of the two stainless steel 316L lattice models revealed the engineering stress-strain response presented in Fig. 11. It was observed that the SCL yielded at a stress level of 74 MPa , while the OTL yielded at a stress value of 49 MPa . The increase in the yield strength is consistent with what expected by analytical solution. Recalling Eq. (11), and using the diameters measured by the polarized light microscope, which are $527 \mu\text{m}$ for the SCL and $473 \mu\text{m}$ for the OTL, the ratio of the yield strength of the SCL to the OTL ($\frac{\sigma_{y12}}{\sigma_{y11}}$) is 1.57 analytically. The experimental results showed almost the same ratio of 1.51 based on the yield values mentioned above.

$$\frac{\sigma_{y12}}{\sigma_{y11}} = \frac{2\sqrt{10}}{5} \left(\frac{D_2}{D_1} \right)^2 = \frac{2\sqrt{10}}{5} \left(\frac{527}{473} \right)^2 = 1.57 \quad \text{Analytically}$$

$$\frac{\sigma_{y12}}{\sigma_{y11}} = \frac{74}{49} = 1.51 \quad \text{Experimentally}$$

Based on the resulting engineering stress-strain response, the OTL has a SEA of 15.2 kJ/kg and EAE of 32.6% . The proposed SCL features a SEA of 19 kJ/kg and 38.4% efficiency. This means that both SEA and

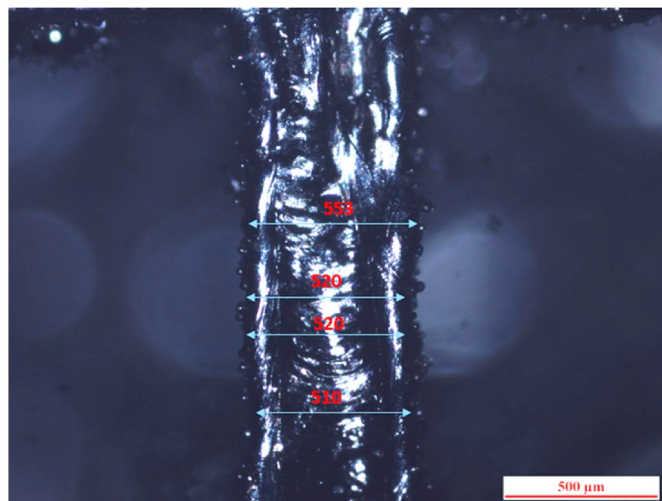


Fig. 9. Polarized light microscope images of a constituent strut of the SCL.

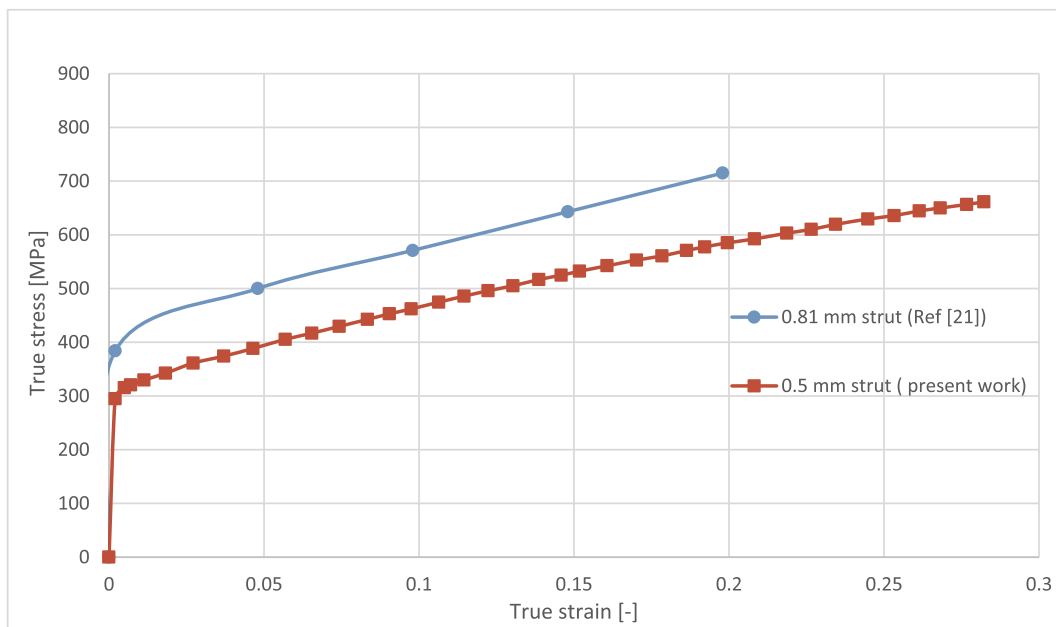


Fig. 10. Basis material stress strain response, obtained from tensile experiments of the 0.5 mm strut, fabricated by SLM with the same process parameters of the fabricated micro-lattices.

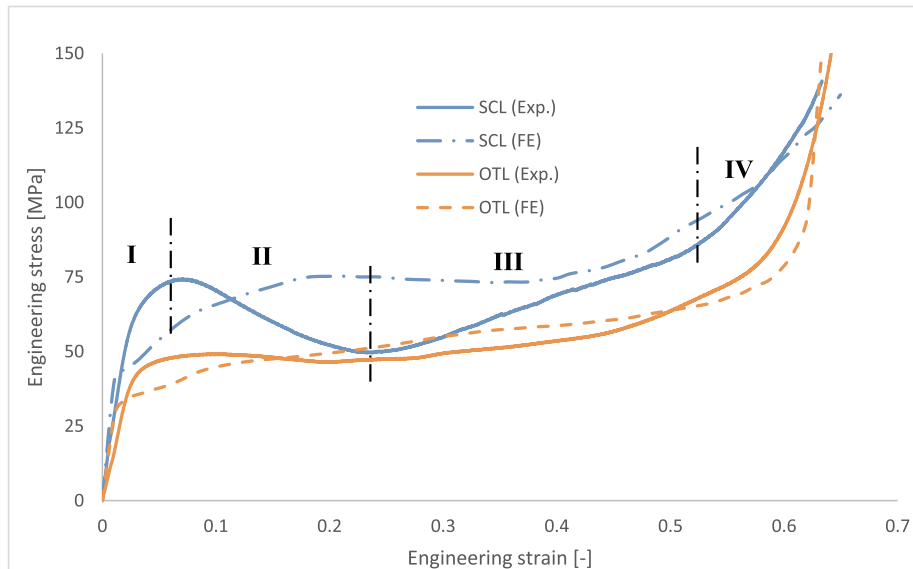


Fig. 11. Macroscopic stress strain response of the SCL and OTL based on quasi-static experiments and FE results.

EAE increased for the SCL by 26% and 17%, respectively compared to the OTL. These results match with the full scale FE model predictions, presented in dotted lines in Fig. 11.

The OTL deforms in a progressive stable crushing mode as shown in Fig. 12. Contrarily, the SCL deforms in an unstable twisting mode as shown in Fig. 13 which was anticipated previously through FE simulations. Four stages are observed during SCL compression, as shown in Figs. 11 and 13: (I) Elastic stage at which the stress increases linearly with strain levels, (II) struts buckling at which twisting mode is observed resulting in a noticeable decline in stress levels, (III) struts collapsing with no more twisting and localized contact between struts occurs which increases stress levels, and finally, full densification takes place at stage (IV).

5.5.2. Composite acrylic-stainless steel metamaterials

The effect of adding acrylic matrix to both stainless steel lattices on the static compression behavior is addressed in Figs. 14 and 15. With regards to the SCL, acrylic enhanced the strut buckling resistance, which resulted in a substantial increase in the lattice strength and a noticeable stress plateau behavior. It is observed in Fig. 16 that the composite SCL deforms in a stable buckling free mode which interprets the resulting stress plateau in Fig. 14 and the disappearance of stress fluctuations revealed in the bare stainless steel SCL. The properties of both SS316L SCL and the composite SCL reinforced by acrylic matrix are summarized in Table 5. It is shown that the hybrid composite SCL offers higher specific strength (47% higher) than that of the stand-alone SCL, while SEA and EAE decreased for the composite SCL by 31.5% and 30.7% respectively. This is attributed to the low densification strains for the composite material due to lack of spacing.

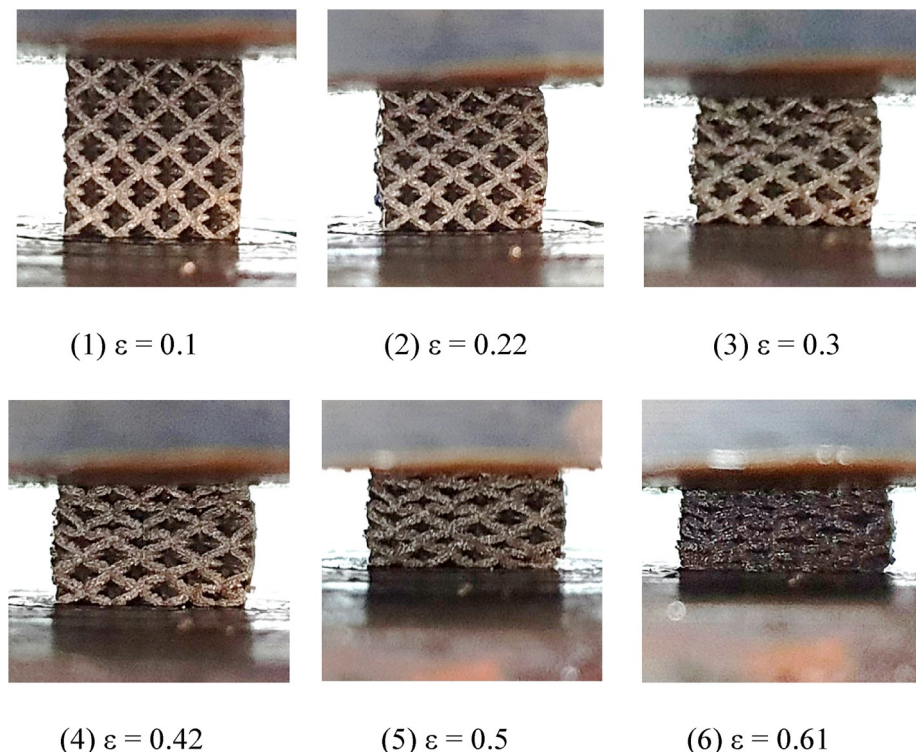


Fig. 12. Selected deformation configurations during quasi-static compression of the OTL.

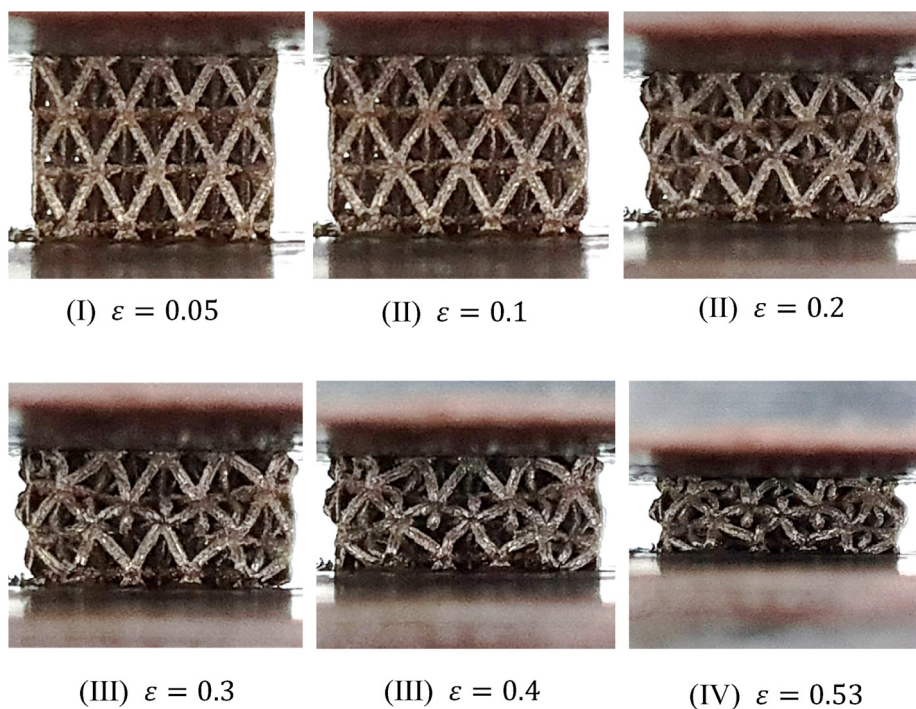


Fig. 13. Selected deformation configurations during quasi-static compression of the SCL.

The acrylic reinforced composite OTL is characterized by higher specific strength (33.6%) compared to the bare SS316L OTL, while the composite OTL suffers from lower SEA (-60.5%) and EAE (-89.5%) than that of the SS316L OTL as shown in **Table 5**. Although adding acrylic to the OTL increased its high specific strength, both SEA and EAE dropped significantly due to the occurrence of densification at low strain levels.

5.6. Dynamic testing of microlattice

5.6.1. Bare stainless steel lattices

The results of the high strain rate compression experiments on the micro-lattice specimens are represented in Fig. 17. The dynamic experiments are carried out at a striker velocity of 22 m/s resulting an average engineering strain rate of 3500/s and 5500/s for the OTL and

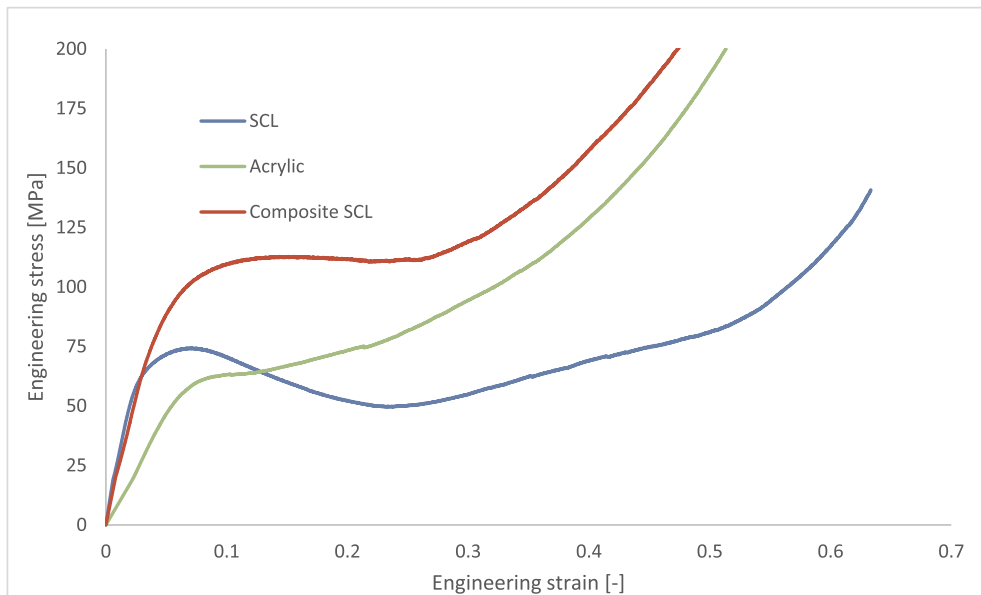


Fig. 14. Macroscopic stress strain response of the SCL, acrylic, and composite SCL.

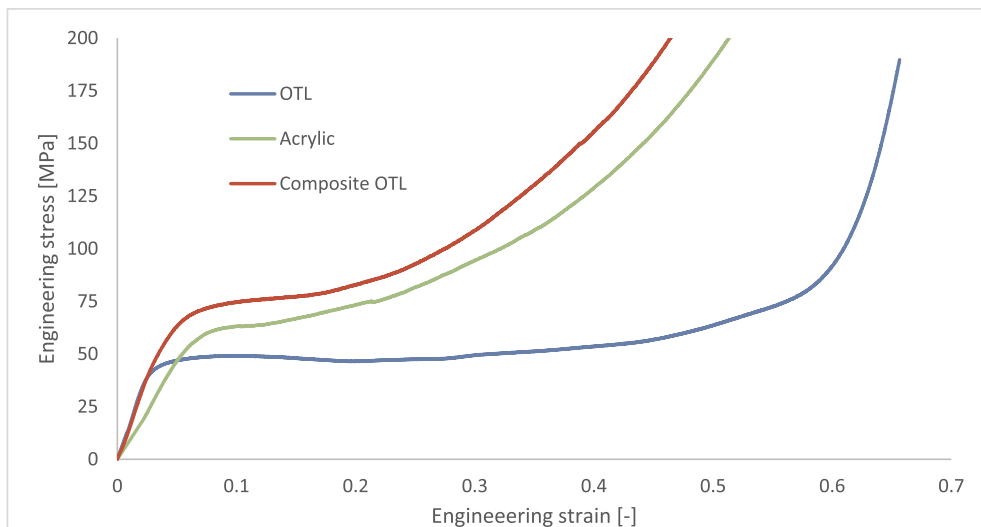


Fig. 15. Macroscopic stress strain response of the OTL, acrylic, and composite OTL.

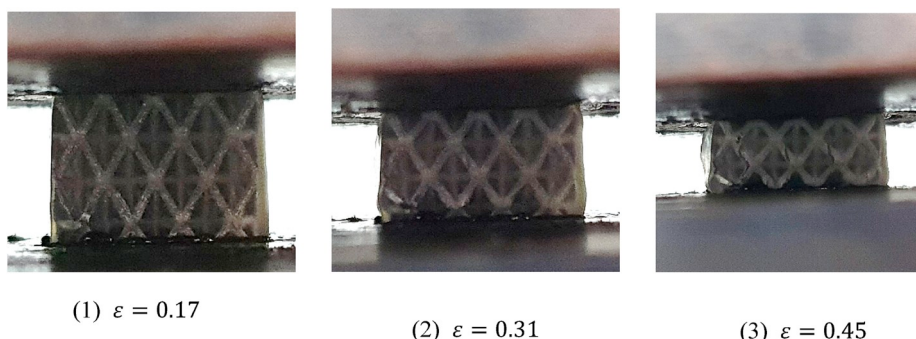


Fig. 16. Selected deformation configurations during quasi-static compression of the composite SCL.

the SCL respectively. The resulting stress strain curves exhibit the same response similar to the quasi-static compression experiments for both models. Dynamic increase factors (DIF) are found to be 1.27 for the OTL

and 1.33 for the SCL, when compared to the quasi-static compression experiments. This is attributed to the DIF of the basis material which was reported by Tancogne-Dejean et al. [21] to be 1.3 for stainless steel 316L

Table 5

Properties of bare SS316L lattices and their corresponding composite acrylic-SS316L lattices based on quasi-static compression experiments.

Property	SCL	Composite SCL	OTL	Composite OTL
Density ρ [g/cm ³]	1.8	2.3	2.17	2.48
Crush strength σ_{crush} [MPa]	60	113	49	75
Specific strength [kN.m/kg]	33.3	49.1 (+47%)	22.6	30.2 (+33.6%)
Densification strain ε_D [-]	0.53	0.3	0.61	0.22
SEA [kJ/kg]	19	13 (-31.5%)	15.2	6 (-60.5%)
EAE [%]	38.4	26.6 (-30.7%)	32.6	17.2 (-89.5%)

fabricated by SLM.

5.6.2. Composite acrylic-stainless steel metamaterials

The engineering stress strain curves resulted from the high strain rate experiments on the plain acrylic and the composite acrylic-stainless steel 316L lattices are depicted in Figs. 18 and 19, respectively, along with

their corresponding quasi-static compressive behavior for comparison. It is observed that plain Quickset acrylic material featured a compressive yield strength of 137 MPa and 65 MPa at strain rate of 7500/s and 10⁻³/s respectively. This corresponds to a DIF of ~2.1 when increasing the strain rate from 10⁻³/s to 7500/s, as shown in Fig. 18. The composite OTL impregnated with acrylic exhibited a dynamic compressive response similar to the static loading curve, i.e. a plateau stress before densification takes place, with a significant DIF of ~2.1 when strain rate increased from 10⁻³/s to 2250/s, see Fig. 19. This could be attributed to the strain rate sensitivity of the Acrylic matrix which revealed the same DIF. This conclusion is emphasized when the noticed DIF for the composite SCL reinforced by Acrylic was observed to be of ~2 (Fig. 19). The composite SCL however revealed a dynamic response different from its static compressive response, where a gradual decrease in the stress level is observed after the initial peak which is attributed to the localized fracture of the constitutive struts of the lattice metamaterial, as presented in Fig. 20.

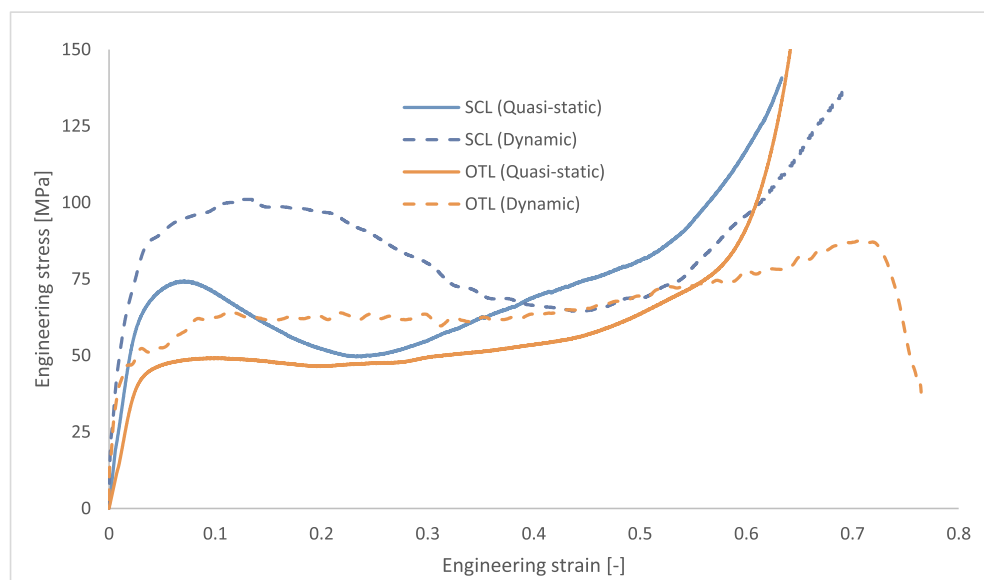


Fig. 17. Quasi-static vs. dynamic compressive response of the OTL and SCL.

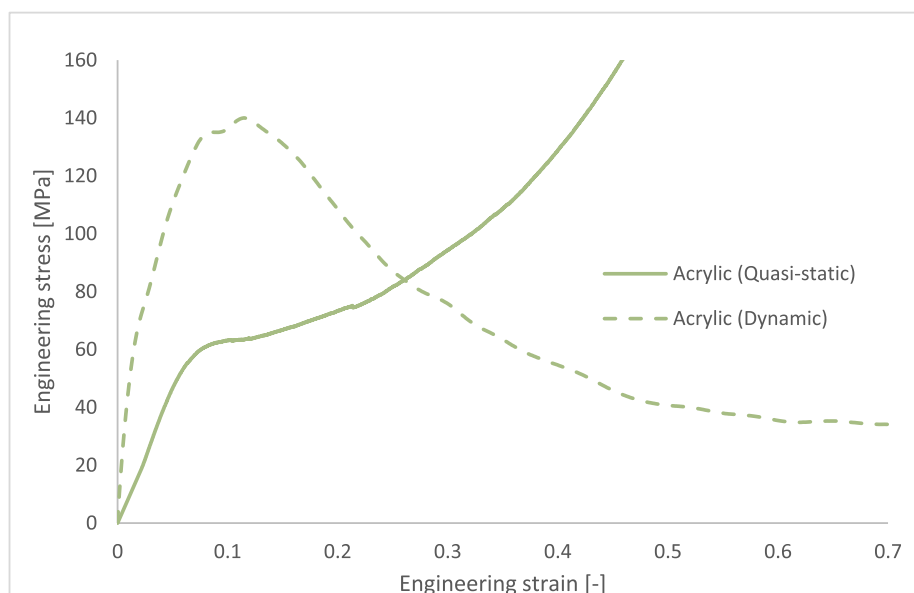


Fig. 18. Static (10⁻³ s⁻¹) vs. dynamic (7500 s⁻¹) compressive response for plain Acrylic.

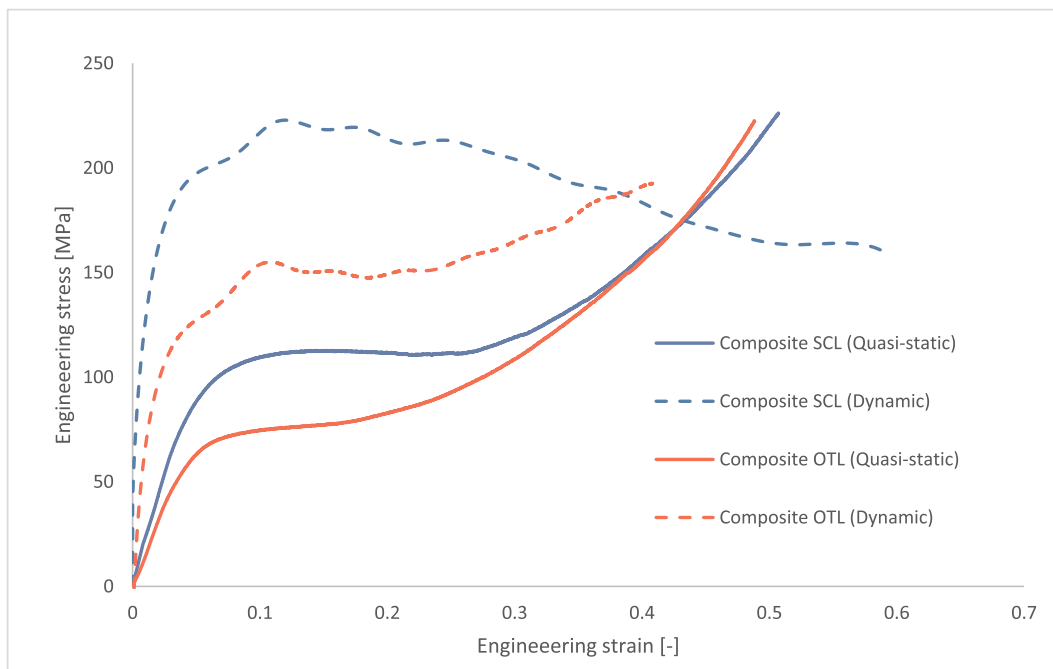


Fig. 19. Static (solid lines) vs. dynamic (dashed lines) compressive response of the composite OTL and composite SCL, at strain rates of 2250/s for the composite OTL and 2750/s for the composite SCL.

Since the DIF of the composite acrylic-stainless steel metamaterial is ~ 2 , while the DIF of the bare stainless steel lattice metamaterial is ~ 1.3 , this leads to a higher increase in strength-to-weight ratio for the hybrid material compared to the bare stainless steel lattices at high strain rates. It was previously mentioned that the increase in the specific strength in case of static loading conditions for the composite SCL and composite OTL was 47% and 33.6% respectively. However, it is demonstrated in Table 6 that the increase in the specific strength is found to be 128% for the composite SCL and 118% for the composite OTL, in case of dynamic loading.

6. Conclusions

In the present work, the quasi-static and dynamic compressive behavior of a new proposed lattice structure, namely SCL, produced by additive manufacturing from Stainless Steel 316L was investigated both numerically and experimentally. In addition, a newly developed composite SCL based on SS 316L and Acrylic matrix has been introduced and evaluated in terms of energy absorption and specific strength under quasi-static and dynamic compression. Finite element simulations and experimental work have led to the following main conclusions:

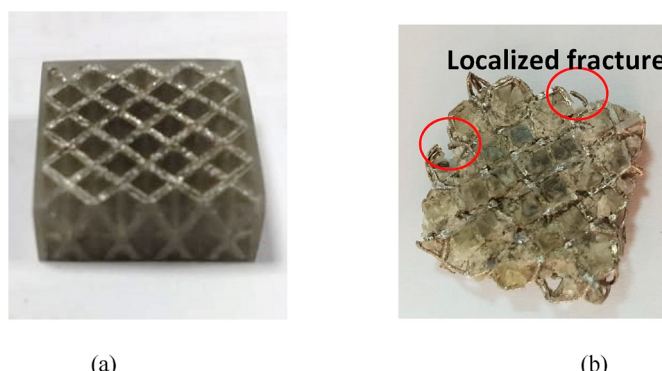


Fig. 20. Composite SCL (a) before and (b) after compression at strain rates of 7500/s, showing localized fracture.

Table 6

Properties of SS316L lattices and their corresponding composite acrylic-SS316L hybrid material based on dynamic compression experiments.

Property	SCL	Composite SCL	OTL	Composite OTL
Density ρ [g/cm ³]	1.8	2.2	2.2	2.5
Crush strength σ_{crush} [MPa]	80	223	62	154
Specific strength [kN.m/kg]	44.4	101.4 (+128%)	28.2	61.6 (+118%)

- 1 A new microlattice architecture was introduced in this study, which is similar to the octet truss lattice (OTL) but with a unit cell aspect ratio of (1:1:2) and is fabricated from stainless steel 316L by selective laser melting (SLM), and is referred to as the stretched cell lattice (SCL). The proposed SCL outperforms the conventional OTL metamaterial in terms of specific energy absorption (SEA) and energy absorption efficiency (EAE).
- 2 The dimensional accuracy of the SLM fabricated microlattice metamaterials depends on the lattice constitutive struts orientation with respect to the build direction. The horizontal struts in the microlattice architectures studied had better dimensional accuracy compared with the 45° inclined struts. The less the inclination angle, the better the accuracy i.e. the constituting struts inclined 26.5° had better dimensional accuracy compared to the 45° inclined struts.
- 3 It was shown analytically that the yield strength of the SCL is $\sim 80\%$ higher than that of the OTL fabricated from the same basis material and of the same relative density, which was confirmed both numerically and experimentally.
- 4 The SCL deforms in an unstable twisting mode under large strain uniaxial compression which is resulted from the buckling of the constituent struts due to their low diameter to length (D/L) ratio, while the OTL deforms in a stable progressive crushing mode.
- 5 Filling the SCL with acrylic, forming a composite SCL, enhanced strut buckling resistance leading to a 47% higher specific strength while the SEA and EAE dropped by 31.5% and 30.7% respectively due to the relatively lower achievable densification strain after adding acrylic.

- 6 Compression experiments at strain rates in the order of 10^3 /s on the bare stainless steel SCL and OTL demonstrated the same macroscopic stress-strain response of static experiments with a dynamic increase factor (DIF) of ~ 1.3 , which is attributed to strain rate sensitivity of the basis material.
- 7 High strain rate experiments on the composite SCL and the composite OTL revealed a DIF of ~ 2 , which was found to be similar to the DIF of the used acrylic. This relatively high strain rate sensitivity for the hybrid material leads to a higher specific strength for the hybrid material (up to 128%) as compared to the bare stainless steel microlattices.

CRediT authorship contribution statement

Mahmoud M. Osman: Conceptualization, Methodology, Software, Investigation, Visualization, Writing - original draft. **Mostafa Shazly:** Software, Validation, Resources, Supervision, Writing - review & editing. **Ehab A. El-Danaf:** Validation, Supervision, Writing - review & editing. **Parastoo Jamshidi:** Investigation. **Moataz M. Attallah:** Validation, Resources.

References

- [1] Zheng X, Lee H, Weisgraber T, Shusteff M. Ultralight, ultrastiff mechanical metamaterials. *Science* 2014;344(6190):1373–8.
- [2] Berger JB, Wadley HNG, McMeeking RM. Mechanical metamaterials at the theoretical limit of isotropic elastic stiffness. *Nature* 2017;543(7646):533–7.
- [3] Turco E, Misra A, Pawlikowski M, dell’Isola F, Hild F. Enhanced Piola-Hencky discrete models for pantographic sheets with pivots without deformation energy: numerics and experiments. *Int J Solids Struct* 2018;147:94–109.
- [4] dell’Isola F, et al. Pantographic metamaterials: an example of mathematically driven design and of its technological challenges. *Continuum Mech Therm* 2019; 31:851–84.
- [5] Barchiesi E, Spagnuolo M, Placidi L. Mechanical metamaterials : a state of the art. *Math Mech Solids* 2019;24(1):212–34.
- [6] Rashed MG, Ashraf M, Mines RAW, Hazell PJ. Metallic microlattice materials: a current state of the art on manufacturing, mechanical properties and applications. *Mater Des* 2016;95:518–33.
- [7] O’Masta MR, Dong L, St-Pierre L, Wadley HNG, Deshpande VS. The fracture toughness of octet-truss lattices. *J Mech Phys Solids* 2017;98:271–89.
- [8] Maskery I, Aboulkhair NT, Aremu AO, Tuck CJ, Ashcroft IA. Compressive failure modes and energy absorption in additively manufactured double gyroid lattices. *Addit. Manuf.* 2017;16:24–9.
- [9] Xiong J, et al. Advanced micro-lattice materials. *Adv Eng Mater* 2015;17(9): 1253–64.
- [10] Ullah I, Brandt M, Feih S. Failure and energy absorption characteristics of advanced 3D truss core structures. *Mater Des* 2016;92:937–48.
- [11] Ozdemir Z, Tyas A, Goodall R, Askes H. Energy absorption in lattice structures in dynamics: nonlinear FE simulations. *Int J Impact Eng* 2017;102:1–15.
- [12] Ozdemir Z, et al. Energy absorption in lattice structures in dynamics: Experiments. *Int J Impact Eng* 2016;89:49–61.
- [13] Mohsenizadeh M, Gasbarri F, Munther M, Beheshti A, Davami K. Additively-manufactured lightweight Metamaterials for energy absorption. *Mater Des* 2018; 139:521–30.
- [14] Li P, Wang Z, Petrinic N, Sivior CR. Deformation behaviour of stainless steel microlattice structures by selective laser melting. *Mater Sci Eng A* 2014;614: 116–21.
- [15] Salari-Sharif L, Valdevit L, Schaedler TA. Energy dissipation mechanisms in hollow metallic microlattices. *J Mater Res* 2014;29(16):1755–70.
- [16] Li SJ, et al. Compression fatigue behavior of Ti-6Al-4V mesh arrays fabricated by electron beam melting. *Acta Mater* 2012;60(3):793–802.
- [17] Al-Saeid DSJ, Masood SH, Faizan-Ur-Rab M, Alomarah A, Ponnusamy P. Mechanical properties and energy absorption capability of functionally graded F2BCC lattice fabricated by SLM. *Mater Des* 2018;144:32–44.
- [18] Li P. Constitutive and failure behaviour in selective laser melted stainless steel for microlattice structures. *Mater Sci Eng A* 2015;622:114–20.
- [19] Vrana TZR, Koutny D, Palousek D. Impact resistance of lattice structure made by Selective Laser Melting from AlSi12 alloy. *MM Sci. J.* 2015;852–5.
- [20] Tancogne-Dejean T, Mohr D. Stiffness and specific energy absorption of additively-manufactured metallic BCC metamaterials composed of tapered beams. *Int J Mech Sci* 2018;141:101–16.
- [21] Tancogne-Dejean T, Spierings AB, Mohr D. Additively-manufactured metallic micro-lattice materials for high specific energy absorption under static and dynamic loading. *Acta Mater* 2016;116:14–28.
- [22] Contuzzi N, Campanelli SL, Casavola C, Lamberti L. Manufacturing and characterization of 18Ni marage 300 lattice components by selective laser melting. *Materials* 2013;6(8):3451–68.
- [23] Harris GJMJA, Winter RE. Impact response of additively manufactured metallic hybrid lattice materials. *Int J Impact Eng* 2017;104:177–91.
- [24] Deshpande VS, Fleck NA, Ashby MF. Effective properties of the octet-truss lattice material. *J Mech Phys Solids* 2001;49(8):1747–69.
- [25] Johnston SR, Reed M, Wang HV, Rosen DW. Analysis of mesostructure unit cells comprised of octet-truss structures. In: Proc. of the The Seventeenth Solid Freeform Fabrication Symposium; 2006. p. 421–32.
- [26] Deshpande VS, Ashby MF, Fleck NA. Foam topology: bending versus stretching dominated architectures. *Acta Mater* 2001;49(6):1035–40.
- [27] Elsayed MSA, Pasini D. Multiscale structural design of columns made of regular octet-truss lattice material. *Int J Solids Struct* 2010;47(14–15):1764–74.
- [28] Ushijima K, Cantwell WJ, Mines RAW, Tsopanos S, Smith M. An investigation into the compressive properties of stainless steel micro-lattice structures. *J Sandw Struct Mater* 2011;13(3):303–29.
- [29] Cluff DRA, Esmaeili S. “Compressive properties of a new metal – polymer hybrid material. *J Mater Sci* 2009;44(14):3867–76.
- [30] Liu Q, Fu J, Ma J, Chen H, Li Q, Hui D. Axial and lateral crushing responses of aluminum honeycombs filled with EPP foam. *Compos. Part B* 2017;130:236–47.
- [31] Zhang Y, Liu Q, He Z, Zong Z, Fang J. Dynamic impact response of aluminum honeycombs filled with Expanded Polypropylene foam. *Compos. Part B* 2019;156: 17–27.
- [32] Campbell JE, Forte F, Hibbard GD, Naguib HE. Periodic cellular metal/polyurethane foam hybrid materials. *J Compos Mater* 2009;43(3):207–16.
- [33] Yungwirth CJ, Radford DD, Aronson M, Wadley HNG. Experiment assessment of the ballistic response of composite pyramidal lattice truss structures. *Compos B Eng* 2008;39:556–69.
- [34] Gümrük R, Mazlum U, Mines RAW. Compressive mechanical behaviors of hybrid composite materials based on micro lattice structure and rubberlike materials. *Rubber Chem. Technol.* 2015;88(1):147–62.
- [35] Schaedler TA, et al. Designing metallic microlattices for energy absorber applications. *Adv Eng Mater* 2014;16(3):276–83.
- [36] Osman MM, Shazly M, El-Danaf E, Jamshidic P, Attallah M. Evaluation of additively-manufactured metallic microlattice structures for energy absorption applications under quasi-static and dynamic Loadings. *J Mech Phys Solids* 2019. submitted for publication.
- [37] Bowman HA, Schoonover RM. Procedure for high precision density determinations by hydrostatic weighing. *J Res Natl Bur Stand* 1967;71(3):179–98.
- [38] Shazly M, Bahei-El-Din Y, Salem S. Characterization of sandwich panels for indentation and impact. *J Phys: Conf Ser* 2013;451:012001.
- [39] Acharya S, Mukhopadhyay A. High strain rate compressive behavior of PMMA. *Polym Bull* 2014;71(1):133–49.
- [40] ASTM A240/A240M-16a. Standard specification for chromium and chromium-nickel stainless steel plate, sheet, and strip for pressure vessels and for general applications. West Conshohocken, PA: ASTM International; 2016. <http://www.astm.org>.